Ocean Dynamics
DOI 10.1007/s10236-017-1042-7

The role of coastal-trapped waves on the 2008 cold disaster in the Taiwan Strait

Enhui Liao[1,2] · **Xiao-Hai Yan**[1,2] · **Yuwu Jiang**[1]

Received: 30 July 2016 / Accepted: 24 February 2017

Abstract In early 2008, cold water in the Taiwan Strait (TWS) was moved sequentially by a cross-strait flow and a southward flow to the Penghu Island, causing a cold-related fish kill disaster. Except for the local wind forcing, the coastal-trapped waves (CTWs), intermittently propagating toward the TWS from north in winter, are an additional factor that could impact the flow patterns by changing cross-strait sea-level gradient during the disaster. In the first stage (January 28–February 7), the reach of a large CTW trough induced an additional northward flow, which formed a cyclone after turning around the Zhangyun Ridge. Then, the cyclone led to an additional cross flow, which enhanced an eastward (offshore) movement of cold water. In the second stage (February 7–14), the arrival of a large CTW crest triggered an additional southward flow, which intensified a southward movement of the cold water. Due to the additional eastward and southward movements caused by the CTWs, the cold water could reach Penghu Island inducing a cold disaster.

Keywords Coastal-trapped waves · Taiwan Strait · Circulation · Cold disaster

Key points
- CTWs induced by remote wind can impact circulation in the Taiwan Strait.
- A CTW trough enhanced cold water offshore transport in the first stage.
- A CTW crest intensified cold water southward intrusion in the second stage.

This article is part of the Topical Collection on the *8th International Workshop on Modeling the Ocean (IWMO), Bologna, Italy, 7-10 June 2016*

Responsible Editor: Guoping Gao

✉ Yuwu Jiang
ywjiang@xmu.edu.cn

[1] State Key Laboratory of Marine Environmental Science, Xiamen University, Xiamen 361005, China

[2] College of Earth, Ocean and Environment, University of Delaware, Newark, DE 19716, USA

1 Introduction

In the La Niña winter (January and February) of 2008, extremely strong northeasterly winds (>6.7 m/s) lasted an exceptional long duration (>30 days) in the Taiwan Strait (TWS, Chang et al. 2009). The strong winds strengthened the China Coastal Current, carrying a large amount of extremely cold water from north into the northwestern TWS (Zhu et al. 2013). An unusual offshore branch of the cold China Coastal Current then moved the cold water to the Penghu Island (PHI), southeastern strait (Liao et al. 2013a). The PHI, well known for its coral reef ecosystem, is generally surrounded by a warming water (>20 °C) in winter (Jan et al. 2006). The unexpected cold water (<16 °C) intrusion induced the temperature-sensitive coral reefs and fish to die around the PHI, resulting in serious mortality to the entire coral reef ecosystem (Hsieh et al. 2008). Similar cold disaster at the PHI occurred four times before 2008 (three times between 1930 and 1934 and once in 1976; Tang 1978).

Normally, the cold offshore branch of the China Coastal Current moves the cold water offshore and turns northward forming a U-turn in the northern TWS (Jan et al. 2002; Li et al. 2006a; Oey et al. 2014). However, Liao et al. (2013a) stated the cold offshore branch, instead of a normally northward turn, unusually flowed southward to the PHI, southern strait in 2008. In detail, during January 28–February 7, a persistent cross-strait flow controlled the TWS and moved the cold water offshore to the central strait. Another strengthened along-

Published online: 28 March 2017

strait flow next dominated the TWS and carried the separated cold water southward to the Penghu Island in February 7–February 14 (PHI, Liao et al. 2013a). The period between January 28 and February 7 is defined as the first stage, and the subsequent period in February 7–February 14 is called the second stage hereafter. As a result, the unexpected cold water intrusion is related to two strengthened flow patterns that follow each other in a particular order. In a normal year, the combination of offshore and southward flows may happen, but the flows are weak and impersistent that cannot move the cold water through the Zhangyun Ridge to the PHI, southern strait (Jan et al. 2002; Li et al. 2006b). Liao et al. (2013a) attributed the strengthened offshore and southward flows to a particular strong local wind stress and a likely weakened northward warm current. However, it is still wondering whether there are any other factors involved in the two unusually strengthened processes besides local forcing.

In winter, the TWS current is driven by two forces in opposing directions, i.e., southward wind stress (northeasterly monsoon) and northward pressure gradient force induced by Kuroshio (Yang 2007). Both two forces interact with each other forming three complex current patterns: the southward (northward) current for northeasterly winds stronger (weaker) than an upper (lower) bound and the cross-strait flow for relaxing northeasterly winds between two bounds (Oey et al. 2014). In contrast with the two aforementioned local factors, Ko et al. (2003) reported a huge influence of coastal-trapped waves (CTWs), generated in the Yellow and East China Sea, on the volume transport of the TWS. A positive (or negative) sea surface height (SSH) anomaly, created by a wind stress event in the Yellow and East China Sea, can propagate southward along the China Coast as the CTWs (Jacobs et al. 1998a; Jacobs et al. 1998b). When the CTWs pass through the East China Sea into the TWS, the CTW crest induces a high sea level and strengthens the southward geostrophic current by changing the cross-strait sea-level gradient (Ko et al. 2003).

The CTWs are characterized by not only a high sea level (wave crest) but also a low sea level (wave trough). Is it possible that the low sea level can strengthen the northward geostrophic current like the high sea level strengthens the southward geostrophic current? The northward warm current, as a counter-wind flow (the monsoon in winter is from northeast), has received strong interests (Ma et al. 2010; Yang 2007). At present, there have been few factors reported that can drive the counter-wind flow except for the Kuroshio. Therefore, it is worth studying the impact of CTWs on the concerned counter-wind flow. If CTWs can impact both the northward and southward current, what is the role of the CTWs played in the cross-strait flow leading to the eastward (offshore) movement of cold water? These questions are going to be studied in this paper.

Yin et al. (2014) indicated that the CTWs, propagating in the East China Sea, have three different modes: the free Kelvin wave mode and the forced first and second shelf wave modes. Their amplitudes are O (10 cm), and periods vary from 2 to 11 days. The sea-level variation of the CTWs mainly results from the Kelvin wave mode, whose phase speeds are about 15–18 m/s (Chen and Su 1987; Li 1989; Wang et al. 1988; Yin et al. 2014). Although there are several studies, involving the generations, mechanisms, and propagation properties, on the CTWs along the China Coast, none of them elaborate the impact of CTWs on the 2008 cold disaster in the TWS.

The objective of this study is to investigate the impacts of CTWs on the circulation during the 2008 cold disaster in the TWS. The paper is organized as follows. The data, method, and model are described in Section 2. The impacts of CTWs on the northward (southward) flow and transport in the TWS are studied in Section 3. The relation between the CTWs and the cold water intrusion is explored in Section 4. The discussion and summary are given in Section 5.

2 Model, data, and method

The model used in the study is a one-way nested model which is based on the Regional Ocean Modeling System (ROMS), a free-surface, hydrostatic, primitive equation ocean circulation model with nonlinear terrain-following coordinates (Shchepetkin and Mcwilliams 2003, 2005). The coarse grid is from the TWS Nowcast/Forecast System (TFOR), which has been an operational forecasting system for the Fujian Province Marine Forecasting Institute since 2003. The TFOR has been extensively assessed and verified by Lin et al. (2016), and the results have been used to study various oceanic phenomena in the TWS (Chen et al. 2014; Liao et al. 2013b; Liao et al. 2015; Lu et al. 2015; Wang et al. 2013). The model spans the northwestern Pacific from 99.0° E to 148° E and 9.0° S to 44.0° N at 1/8° horizontal resolution with 25 vertical levels. The fine-grid model covers the TWS from 111.4° E to 125.2° E and 14.5° N to 28.4° N at 1/32° horizontal resolution with 25 vertical levels. The model bathymetry is a combination of survey data and ETOPO2v2 from National Geophysical Data Center (http://www.ngdc.noaa.gov/mgg/fliers/01mgg04.html). The air-sea flux data (heat and mass) and wind forcing for both nested grids are from MERCATOR PSY3V2R2 (http://www.mercator-ocean.fr, 2008). The initial and lateral boundary conditions of the fine-grid model are interpolated from the results of the coarse-grid model. In addition, the major rivers' discharge along the coast and sea level forced by 10 main tidal components are included in the lateral boundary condition.

The default schemes in the ROMS are adopted to resolve horizontal and vertical advection terms of momentum and tracer equation in the fine-grid model (third-order upstream bias and fourth order centered for horizontal and vertical advections of 3D momentum, respectively, fourth order centered

for 2D momentum and traces' equation). The Smagorinsky diffusion is used for the harmonic horizontal mixing of tracers, which occurs along the geopotential surface. The vertical viscosity and diffusion rates are calculated by the MY2.5 turbulence module. The Flather scheme is employed for the radiation boundary condition (Flather 1987). The tidal processes are added to the model by the Chapman boundary condition (Chapman 1985). The other model configurations and validations are detailed in Liao et al. (2013a) and Lin et al. (2016).

The CTWs originated in the Yellow and East China Sea and transported into the TWS through sea level and velocity variability. The coarse-grid domain covers the whole area, and the fine-grid domain only focuses on the TWS. The CTWs are generated in the coarse-grid model and transport into the fine-grid model through boundary conditions, i.e., sea level and velocity. Therefore, the CTWs' transport into the TWS can be controlled by filtering the sea level and velocity variability in the north lateral boundary of the fine-grid model. In order to investigate the role of CTWs in the circulation during the cold disaster, a sensitive numerical test (non-CTW case, here after) was performed in the fine grid from 30 December 2007 to 20 March 2008. The only difference between control and non-CTW case is the north lateral boundary condition. For the control case, the north lateral boundary conditions were interpolated from coarse-grid model without any change. For the non-CTW case, the north lateral boundary conditions, i.e., sea level and velocity, were interpolated from the coarse-grid model and then were filtered with a low-pass filter. The CTW periods vary from 2 to 11 days in the East China Sea (Yin et al. 2014), where the north boundary of the fine grid is located. Therefore, in the north boundary of the non-CTW case, the momentums (sea level and velocities in 2D and 3D), temperature, and salinity were filtered by a 15-day low-pass filter to remove the CTW signals entering the model from the north. The other three lateral boundary conditions and surface forcing, e.g., wind stress, surface heat flux, and surface mass flux, are the same in the control and non-CTW cases. The control case includes two factors: local wind stress and remote CTWs, while the non-CTW case only includes local wind stress. Note that the wind stress in 2008 is much stronger than the wind stress in a normal year. The non-CTW case is not a normal case, but a special case with an extremely strong local wind.

The hourly velocities, measured by an acoustic Doppler current profile (ADCP) buoy (location is shown in Fig. 1), were used to compute the wave frequency during the cold disaster. The buoy was included in the Fujian Coastal Monitored System Project and is used in the monitoring system at the Fujian Marine Forecasts Institute (http://www.fjmf.gov.cn/OceanObservation/BigBuoy.aspx, 2014). The measured depth is from 5.5 to 50.5 m with a vertical resolution of 5 m. The 36-h low-pass-filtered depth-mean

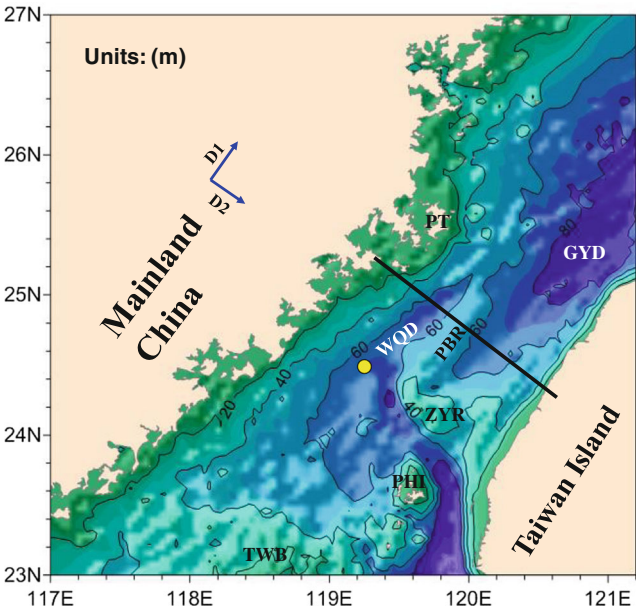

Fig. 1 The seafloor in the Taiwan Strait. *D1* and *D2* are the along-strait and cross-strait directions, respectively. *PT*, *PHI*, *TWB*, *ZYR*, *PBR*, *WQD*, and *GYD* denote the Pingtan, Penghu Island, Taiwan Bank, Zhangyun Ridge, Pengbei Ridge, Wuqiu Depression, and Guanyin Depression, respectively. The *yellow dot* represents the buoy's location. The *black straight line* is the cross-strait section used for volume transport calculation

velocities are used and rotated to the cross-strait and along-strait directions.

The ensemble empirical mode decomposition (EEMD) method is applied to analyze the frequency (Hilbert spectrum) of buoy velocities. This is an adaptive method which decomposes a time series into a set of intrinsic mode functions and a residual monotonic function through a sifting process. The EEMD can overcome the mode mixing problem in the empirical mode decomposition (Huang et al. 1998). The EEMD scheme can extract physically meaningful modes from a non-stationary and nonlinear time series and thus has been widely used in oceanography (Ezer et al. 2013; Li et al. 2012; Yin et al. 2014). The Hilbert spectrum can be calculated by applying Hilbert transform after obtaining the intrinsic mode functions.

3 The impact of CTWs on the northward and southward flow

The major characteristics of SSH anomaly (tide-filtered SSH minus monthly mean SSH) were notably low and high sea levels in the TWS during the first and second stage, respectively (Fig. 2). Eight panels of SSH anomaly at different times demonstrate an excitation and transportation of the low and high sea levels from the Yellow Sea to the TWS along the China Coast. For the low SSH anomaly event, sea level fell with a weak wind stress in the Yellow Sea on February 3 and

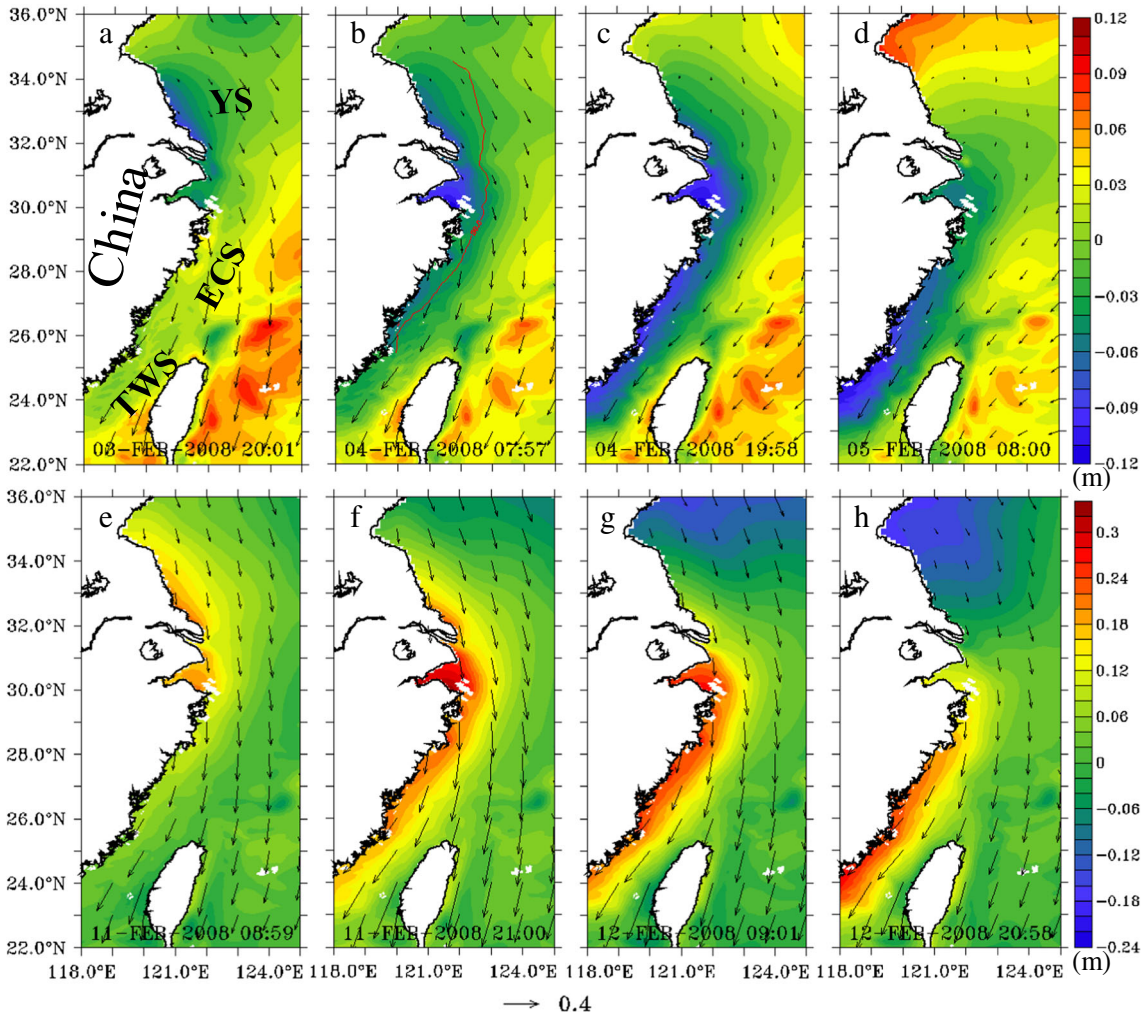

Fig. 2 The simulated 12-hourly sea-level anomaly (tidal-filtered sea level minus the monthly mean sea level) along the China Coast. The low and high sea level propagated southward on February 3 (*upper panel*) and February 11 (*lower panel*), respectively. The MERCATOR wind stress vectors (unit: N/m^2) are superimposed. In **a**, the *YS*, *ECS*, and *TWS* represent Yellow Sea, East China Sea, and Taiwan Strait, respectively. In **b**, the *red line* is the isobaths of 30 m along the China Coast

then propagated southward through the East China Sea to the TWS in 1 day. For the high SSH anomaly event, sea level rose with a strong wind stress in the Yellow Sea on February 11 and then transported southward. The high sea level also took almost 1 day to transport from the Yellow Sea to the TWS. Note that the coast is located to the right of the propagation direction.

The time series of the SSH anomaly along the 30-m isobath (the isobath is shown in Fig. 2b) is plotted in Fig. 3a. The figure illustrates propagations of low and high sea levels from north to south, which coincided well with Fig. 2. According to the propagation distance and period (Fig. 3a), the propagation speed is estimated to be 16.8 m/s, which almost equals the phase speed of long surface gravity wave in 30-m depth. The speed approximates to the phase speed of the first mode of CTWs (Kelvin wave) reported in CTW studies along the China Coast as well (Chen and Su 1987; Yin et al. 2014).

Figure 3b displays Hilbert spectrum (calculated by EEMD) of the velocities monitored by the buoy in the TWS. The lines represent the high spectra with time. The variation suggests a fluctuation of frequency for nonlinear effect. The spectrum indicated two primary frequencies of about 0.4 and 0.1 cycles per day (cpd) between February 3 and 5 (the arrival of the CTW trough) and three primary frequencies of about 0.3, 0.2, and 0.1 cpd between February 11 and 12 (the arrival of the CTW crest). These frequencies are similar to the frequencies of previous CTW studies (Li 1989; Yin et al. 2014), e.g., the frequencies range from 0.09 to 0.5 cpd. The transport direction, estimated phase speed, and wave frequencies are consistent with previous CTW studies along the China Coast. This indicates the waves can be considered as barotropic coastal-trapped Kelvin waves.

Time series of cross-strait sea-level difference between the control and non-CTW cases are illustrated in Fig. 4a. The sea-

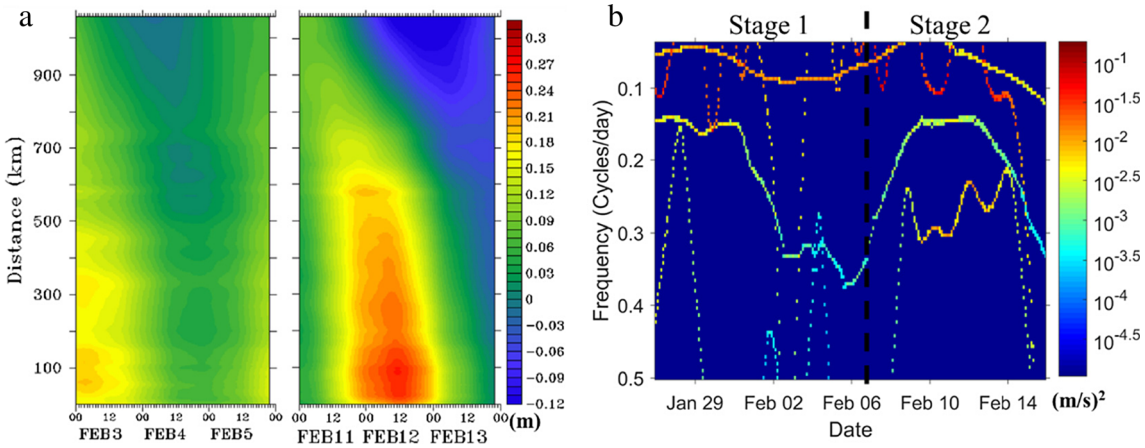

Fig. 3 The time-distance plot of the alongshore sea-level anomaly (tidal-filtered sea level minus the monthly mean sea level, **a**) and Hilbert spectrum of vertical averaged velocity of the buoy (**b**). In **a**, the distance is from Taiwan Strait toward the Yellow Sea along the 30 m isobaths (plotted in Fig. 2). The low and high sea level originated in the Yellow Sea and propagated southward along the isobaths

level difference can be treated as the sea level caused by the CTWs. The negative and positive values appeared alternatively with time. This means wave trough and crest propagated from the north toward the TWS continually (Fig. 4a). The Rossby deformation radius (280 km) in this region is larger than the strait width (about 200 km) in the TWS. This suggests the sea level, generated by the CTWs, can modify the cross-strait sea-level gradient. The strongest negative (positive) values emerged on February 4 (February 12), which matched the arrival time of the wave trough (crest) shown in Figs. 2 and 3.

Ko et al. (2003) showed the dominant dynamics, governing the volume transport through the TWS in the winter, is in geostrophic balance when the water is well mixed. Although the phase speed of CTWs is very fast (16.8 m/s), the wave length of CTWs is very long (~1000 km). Therefore, the passage time is about 20 h, which is larger than the geostrophic adjustment time ($\sim f^{-1}$, ~4.5 h) in the TWS. This suggests the high and low sea levels can remain in the TWS for enough time to induce geostrophic flow. Therefore, the volume transport caused by the CTWs can be estimated by the cross-strait sea-level difference. The along-strait geostrophic current can be calculated by $v = \frac{g}{f}\frac{\partial \eta}{\partial x}$, and the volume transport can be estimated by

$$Sv = \frac{10^{-6} g h \Delta \eta}{f} \quad (1)$$

where f is Coriolis coefficient (6.048×10^{-5} s^{-1}), g is gravity acceleration constant, h is averaged depth along the cross-strait section (50 m), $\Delta\eta$ is cross-strait sea-level differences (can be estimated from Fig. 4a), Δx is width of the cross-strait section (175 km), and v is along-strait velocity.

Figure 4b shows time series of the volume transport through the TWS. The red dot line (non-CTWs + CTWs) is the sum of the transport in the non-CTW case (green dashed line) and the transport estimated by Eq. 1 (generated by the CTWs). The sum transport (non-CTWs + CTWs) is almost similar to the transport of the control case (black dashed line). This suggests the transport differences between these two cases were caused by the CTWs. Specifically, the wave crest (trough) could induce a negative (positive) cross-strait sea-level gradient through increasing (decreasing) the sea level in the western strait. The negative (positive) cross-strait sea-

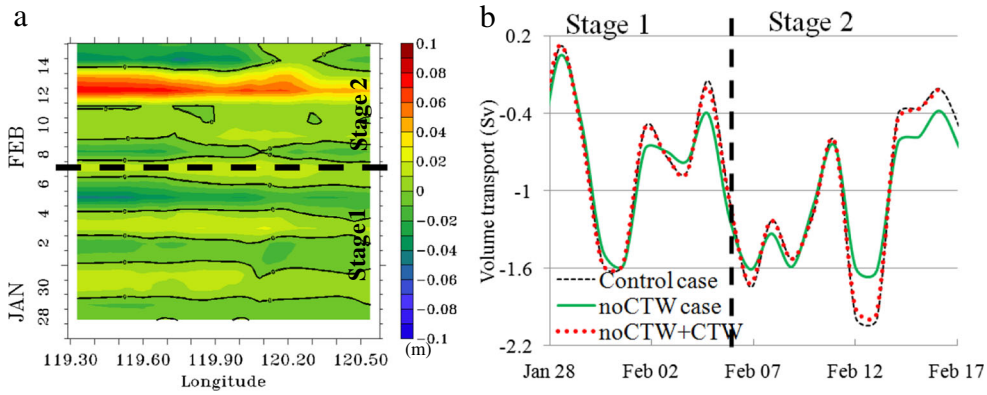

Fig. 4 The cross-strait sea-level difference (the control case minus non-CTW case, **a**) and volume transport (**b**, unit: Sv, $\times 10^6$ m^3/s) through a section in the Taiwan Strait. The position of the section is shown in Fig. 1. The *red dot line* in **b** is the sum of non-CTW case and the transport induced by the CTWs (estimated by Eq. 1)

level gradient can strengthen a southward (northward) geostrophic current leading to an increased southward (northward) volume transport.

The large transport differences between the control and non-CTW cases emerged on February 4 and 12, which are consistent with the arrival times of the wave trough and crest, respectively (Fig. 4b). On February 4, the CTW trough decreased the southward transport from −0.40 to −0.14 Sv through weakening the mean southward current by 0.03 m/s. In other words, the wave trough increased the northward transport by 0.26 Sv through strengthening the northward flow by 0.03 m/s. On February 12, the wave crest changed the volume transport from −1.61 to −1.99 Sv through intensifying southward geostrophic current from 0.18 to 0.23 m/s. This means the CTW crest could increase the southward transport by 0.38 Sv on February 12.

In summary, a large CTW trough (crest), occurred in the first (second) stage, strengthened the northward (southward) geostrophic current and northward (southward) volume transport through changing the cross-strait sea-level gradient. Note that there was a huge impact of the CTWs on the volume transport in 2008, and similar impact can be found in other years as well (Ko et al. 2003). This indicates the CTWs may play an important role in short-term variation of volume transport in the TWS.

4 Coastal-trapped waves and intensified cold water intrusion

The PHI, located in the southeastern TWS, is surrounded by a warm water from the south almost all through the year (Jan et al. 2006; Liao et al. 2013a). The huge temperature decrease around the PHI in 2008 was induced by the unique dynamic processes (Liao et al. 2013a), which are affected not only by the local wind stress but also by the CTWs. Figure 5 illustrates the time series of temperature (Zhangyun Ridge and PHI) and the CTW propagation. The temperature at the Zhangyun Ridge decreased largely from January 28 to February 7 (the first stage) and increased on February 7–14 (the second stage). The temperature at PHI remained constant around February 4 and decreased significantly after February 7. In the first stage, the decreased temperature at Zhangyun Ridge and constant temperature at PHI coincided with eastward movement of cold water that the separated cold water was moved to the Zhangyun Ridge and did not affect the PHI. In the second stage, the increased temperature at Zhangyun Ridge and decreased temperature at PHI matched the southward movement of cold water that the separated cold water left Zhangyun Ridge and transported to PHI. Comparison between the control and non-CTW cases displays the temperature in the first case decreased more than that in the second case. The temperature difference at the Zhangyun Ridge (PHI) happened in

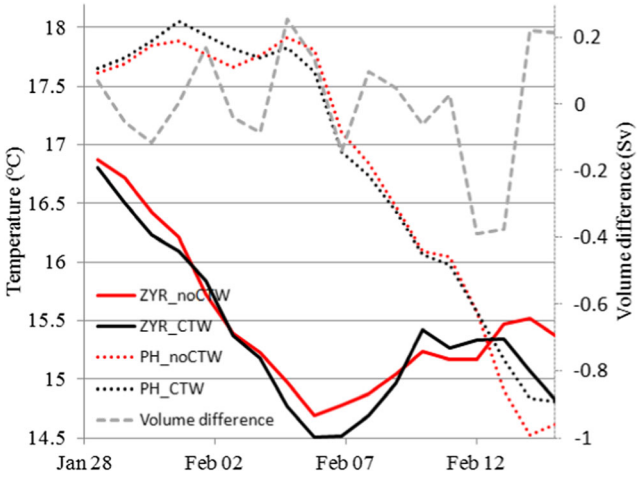

Fig. 5 The time series of temperature at the Zhangyun Ridge and Penghu Island from model results. The *black* (*red*) *line* is the control (non-CTW) case. The *solid* (*dashed*) *line* is the temperature at the Zhangyun Ridge (Penghu Island). The *gray dashed line* is the volume difference between the control case and non-CTW cases. The volume difference is positive (negative) when the wave trough (crest) arrives

February 4–6 (February 12–14) which was the arrival time of the CTW trough (crest). This indicates the temperature differences at Zhangyun Ridge and PHI are related to the CTWs.

In order to show a detailed relation between the CTWs and the temperature differences, the time series of the CTW propagation and the boundaries of separated cold water are displayed in Fig. 6. The boundary of separated cold water is determined by 14.5 °C isotherm. The movement of east (south) boundary can indicate the strength of cross flow (southward flow) which can be affected by the CTW trough (crest). Before the arrival of the CTWs, the east (south) boundaries between the control and non-CTW cases were almost located at the same longitude (latitude, Fig. 6). Around February 4, the transport difference (the control case minus the non-CTW case) increased from −0.01 to 0.25 Sv, suggesting the arrival of the CTW trough. Meanwhile, the east boundary of cold water was moved eastward (120.3° E) in the control case, while it nearly remained at the same place (120.22° E) in the non-CTW case. This indicates the further eastward movement (~8.0 km) in the control case is related to the CTW trough. In February 11–14, the volume difference decreased from −0.01 to −0.39 Sv suggesting the arrival of the CTW crest. The south boundary only reached as south as 23.78° N in the non-CTW case, while it arrived at 23.61° N in the control case. This suggests the further southward movement (~18.9 km) of the cold water was caused by the CTW crest.

Figure 7a, b reveals the positions of 14.5 °C isotherm on February 7 (the end of the first stage) and 14 (the end of the second stage) after the arrival of the CTW trough and crest, respectively. In Fig. 7a, the black line (control case) is ~8.0 km east of the red line (non-CTW case) meaning an enhanced

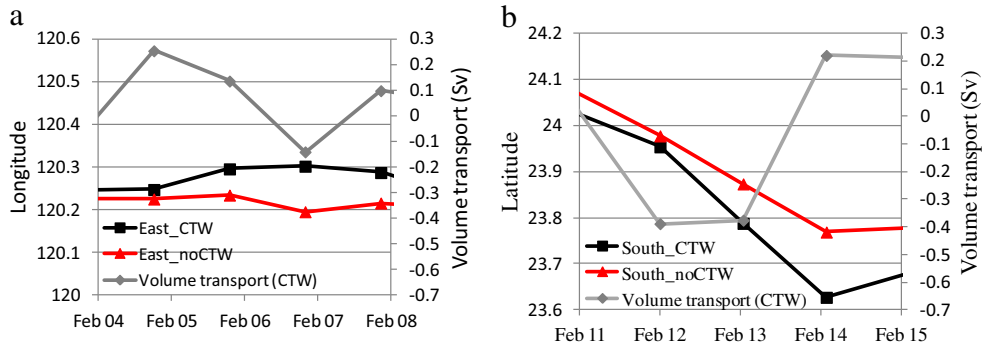

Fig. 6 The time series of east (**a**) and south (**b**) boundary of the separated cold water (indicated by 14.5 °C) in the Taiwan Strait. The *gray line* is the volume difference between the control case and non-CTW cases. The volume difference is positive (negative) when the wave trough (crest) arrives. The *black line* is the boundary position in the control case, and the *red line* is the boundary position in the non-CTW case

eastward movement of cold water induced by the CTW trough. In Fig. 7b, the black line is ~18.9 km south of the red line, indicating an intensified southward movement of the cold water caused by the CTW crest.

In order to study the dynamic mechanism of the additional movement, the sea level and current patterns induced by the CTWs (control case minus non-CTW case) are plotted in Fig. 7c, d. During the first stage, the dominant flow was a cross-strait flow under moderate northeasterly winds (Liao et al. 2013a). The arrival of the CTW trough caused a positive cross-strait sea-level gradient by decreasing the sea level in the western strait (Fig. 7c). The positive cross-strait sea-level gradient induced an additional northward flow which turned around Zhangyun Ridge forming a cyclone in the north of Zhangyun Ridge (Fig. 7c). Oey et al. (2014) shown that a cyclone here contributes to a strongly negative vorticity which results in a cross flow. Therefore, it is the additional cross flow induced by the CTW trough and related cyclone that intensified the eastward (offshore) movement of the cold water. Note that the condition for the additional cross flow caused by the CTW trough is a moderate wind (0.068–0.12 N/m^2, referred to Oey et al. 2014). The impact of the CTW trough on the eastward (offshore) movement of the cold water may be not so significant if the northeasterly wind is beyond the bounds of moderate wind (the corresponding flow pattern is a strong northward/southward flow).

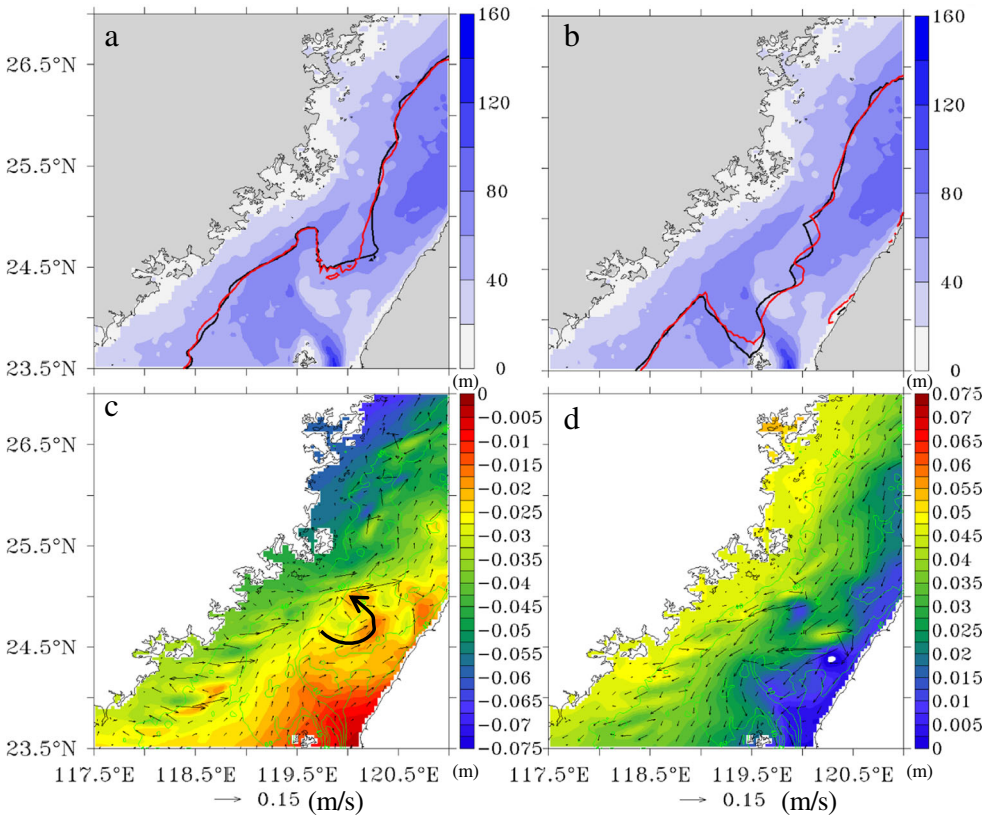

Fig. 7 The position of 14.5 °C isotherm (**a**, **b**) and the sea level and flow differences (**c**, **d**) after the arrival of the CTW trough (**a**, **c**) and crest (**b**, **d**). The difference is the result in the control case minus the result in the non-CTW case. The *black* and *red lines* in **c** and **d** are the control case and non-CTW case, respectively. The *background shadings* (**a**, **b**) and *green lines* (**c**, **d**) show the bottom topography (unit: m). The *anti-clockwise arrow* denotes the cyclonic eddy caused by northward flow

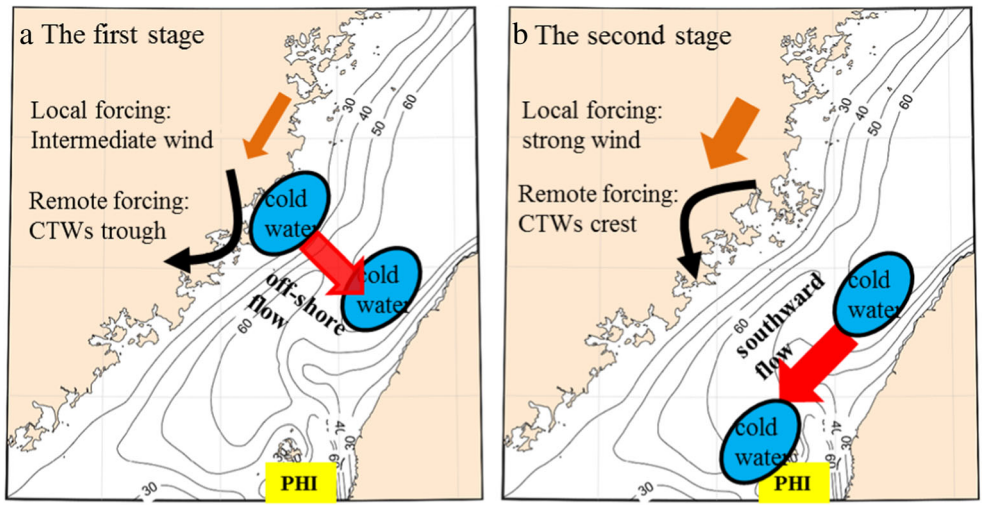

Fig. 8 The schematic diagrams illustrating the processes of cold disaster. **a** The offshore movement caused by the intermediate wind and CTW trough. **b** The southward movement caused by the strong wind and CTW crest. The wind is referred to as the local forcing, and the CTWs are remote forcing

During the second stage, the flow was southward with strong northeasterly winds (Liao et al. 2013a). The arrival of the CTW crest on February 12 generated a negative cross-strait sea-level gradient through increasing the sea level in the western strait (Fig. 7d). The negative cross-strait sea-level gradient induced an additional southward flow through geostrophic balance (Fig. 7d). Therefore, it is the additional southward current caused by the CTW crest that intensified the southward movement of cold water.

In a word, the CTW trough made contribution to the cross flow, and the CTW crest could enhance the southward flow during the first and second stage, respectively. The additional cross flow and southward flow intensified the eastward and southward movements of cold water, respectively. A schematic figure of the dynamic processes is shown in Fig. 8. From the model results in Fig. 7, if the CTWs were removed, the cold water (14.5 °C) cannot reach the PHI and the cold disaster may be avoided. This suggests the additional movements caused by the proceeding CTW trough and crest are critical for the occurrence of cold disaster.

5 Conclusion

In winter, the CTWs, as the third factor, constantly propagating toward the TWS from north, can impact flow patterns in the TWS. The arrival of a CTW trough (crest) in the western coast can strengthen a northward (southward) geostrophic current through changing the cross-strait sea-level gradient. The strengthened northward (southward) current can amplify a northward (southward) volume transport.

During the first stage, the northeasterly wind was moderate resulting in a cross-strait flow pattern. Around February 4, the arrival of a CTW trough induced an additional northward flow. When the northward flow turned around the Zhangyun Ridge, a cyclone was formed in the north of Zhangyun Ridge. This cyclone led to an additional cross flow, which intensified the eastward (offshore) movement of cold water. In the second stage, the northeasterly wind was very strong leading to a southward flow pattern. The reach of a CTW crest generated an additional southward current which increased the southward movement of cold water. The additional eastward and southward flow caused by the CTWs played an important role in transporting the cold water toward PHI killing the tropical fishes there.

The impact of volume transport variations caused by CTWs in the TWS on other ocean phenomena is also worthy to investigate. For example, the volume transport in the TWS is southward (northward) in winter (summer) for northeasterly (southwesterly) monsoon. Moon and Hirose (2014) showed that the seasonal transport variation in the TWS can impact the Kuroshio water intrusion in the East China Sea. Therefore, it is worth to study if the short-term transport variation caused by CTWs can impact the Kuroshio water intrusion in the East China Sea.

Acknowledgements This work was supported by grant 41476005 from the Natural Science Foundation of China (NSFC), grant U1305231 from both NSFC and Fujian Province, grant 2013CB955704 from the National Basic Research Program of China, and grant 2013BAB04B00 from National Key Technology Support Program.

References

Chang Y, Lee KT, Lee MA, Lan KW (2009) Satellite observation on the exceptional intrusion of cold water in the Taiwan Strait. Terr Atmos Ocean Sci 20:661–669

Chapman DC (1985) Numerical treatment of cross-shelf open boundaries in a barotropic coastal ocean model. J Phys Oceanogr 15:1060–1075

Chen DK, Su JL (1987) Continental shelf waves study along China Coast (in Chinese). Acta Oceanol Sin 9:1–15

Chen Z, Yan X-H, Jiang Y (2014) Coastal cape and canyon effects on wind-driven upwelling in northern Taiwan Strait. J Geophys Res Oceans 119:4605–4625

Ezer T, Atkinson LP, Corlett WB, Blanco JL (2013) Gulf Stream's induced sea level rise and variability along the U.S. mid-Atlantic coast. J Geophys Res Oceans 118:685–697

Flather RA (1987) A tidal model of the Northeast Pacific. Atmosphere-Ocean 25:22–45

Hsieh HJ, Hsien YL, Jeng MS, Tsai WS, Su WC, Chen CA (2008) Tropical fishes killed by the cold. Coral Reefs 27:599–599

Huang NE, Shen Z, Long SR, Wu MC, Shih HH, Zheng Q, Yen NC, Tung CC, Liu HH (1998) The empirical mode decomposition and the Hilbert spectrum for nonlinear and non-stationary time series analysis. Proceedings of the Royal Society A: Mathematical, Physical and Engineering Sciences 454:903–995

Jacobs GA, Preller RH, Riedlinger SK, Teague WJ (1998a) Coastal wave generation in the Bohai Bay and propagation along the Chinese Coast. Geophys Res Lett 25:777–780

Jacobs GA, Teague WJ, Riedlinger SK, Preller RH, Blaha JP (1998b) Sea surface height variations in the Yellow and East China Seas-2. SSH variability in the weekly and semiweekly bands J Geophys Res Oceans 103:18479–18496

Jan S, Wang J, Chern CS, Chao SY (2002) Seasonal variation of the circulation in the Taiwan Strait. J Mar Syst 35:249–268

Jan S, Sheu DD, Kuo HM (2006) Water mass and throughflow transport variability in the Taiwan Strait. J Geophys Res Oceans 111:C12012

Ko DS, Preller RH, Jacobs GA, Tang TY, Lin SF (2003) Transport reversals at Taiwan Strait during October and November 1999. J Geophys Res Oceans 108:3370

Li L (1989) A study of winter subtidal sea level fluctuation in the Taiwan Strait. Acta Oceanol Sin 11:275–283

Li C, Hu J, Jan S, Wei Z, Fang G, Zheng Q (2006a) Winter-spring fronts in Taiwan Strait. J Geophys Res 111

Li CY, Hu JY, Jan S, Wei ZX, Fang GH, Zheng QN (2006b) Winter-spring fronts in Taiwan Strait. J Geophys Res 111:C11S13. doi:10.1029/2005jc003203

Li F, Jo Y-H, Liu WT, Yan X-H (2012) A dipole pattern of the sea surface height anomaly in the North Atlantic: 1990s–2000s. Geophys Res Lett 39

Liao EH, Jiang YW, Li L, Hong HS, Yan XH (2013a) The cause of the 2008 cold disaster in the Taiwan Strait. Ocean Model 62:1–10

Liao EH, Jiang YW, Yan XH, Chen ZY, Wang J, Zhang LP (2013b) Allocation of marine environmental carrying capacity in the Xiamen Bay. Mar Pollut Bull 75:21–27

Liao EH, Lu WF, Yan X-H, Jiang YW, Kidwell A (2015) The coastal ocean response to the global warming acceleration and hiatus. Sci Rep 5:16630

Lin X, Yan X-H, Jiang Y, Zhang Z (2016) Performance assessment for an operational ocean model of the Taiwan Strait. Ocean Model 102:27–44

Lu W, Yan X-H, Jiang Y (2015) Winter bloom and associated upwelling northwest of the Luzon Island: a coupled physical-biological modeling approach. J Geophys Res Oceans 120:533–546

Ma C, Wu D, Lin X, Yang J, Ju X (2010) An open-ocean forcing in the East China and Yellow seas. J Geophys Res 115:C12056

Moon J-H, Hirose N (2014) Seasonal response of the southern East China Sea shelf water to wind-modulated throughflow in the Taiwan Strait. Prog Oceanogr 121:74–82

Oey LY, Chang YC, Lin MC, Chang S, Varlamov YM (2014) Cross flows in the Taiwan Strait in winter. J Phys Oceanogr 44:801–817

Shchepetkin AF, Mcwilliams JC (2003) A method for computing horizontal pressure-gradient force in an oceanic model with a non-aligned vertical coordinate. J Geophys Res Oceans 108:3090

Shchepetkin AF, Mcwilliams JC (2005) The regional oceanic modeling system (ROMS): a split-explicit, free-surface, topography-following-coordinate oceanic model. Ocean Model 9:347–404

Tang HG (1978) The situations and reciews of the mass mortalities due to freeze during winter time in Pescadores (in Chinese). China Fish Mon 302:24–26

Wang J, Yuan YL, Pan ZD (1988) Numerical studies and analysis about continental shelf waves (in Chinese). Acta Oceanol Sin 10:666–677

Wang J, Hong H, Jiang Y, Chai F, Yan X-H (2013) Summer nitrogenous nutrient transport and its fate in the Taiwan Strait: a coupled physical-biological modeling approach. J Geophys Res Oceans 118:4184–4200

Yang JY (2007) An oceanic current against the wind: how does Taiwan Island steer warm water into the East China Sea? J Phys Oceanogr 37:2563–2569

Yin L, Qiao F, Zheng Q (2014) Coastal-trapped waves in the East China Sea observed by a mooring array in winter 2006. J Phys Oceanogr 44:576–590

Zhu D, Li L, Guo X (2013) Seasonal and interannual variations of surface current in the southern Taiwan Strait to the west of Taiwan Shoals. Chin Sci Bull 58:4171–4178